QCD-Motivated Pomeron and High Energy Hadronic Diffractive Cross Sections.

V.V.Anisovich[1)], L.G.Dakhno[2)] and V.A.Nikonov[3)]

St.Petersburg Nuclear Physics Institute,
Gatchina, St.Petersburg 188350, Russia
[1)] anisovic@lnpi.spb.su
[2)] dakhno@hep486.pnpi.spb.ru
[3)] nikon@rec03.pnpi.spb.ru

Abstract

Soft diffractive cross sections in pp (or $\bar{p}p$), πp and γp collisions are calculated using QCD-motivated pomeron. The s-channel unitarization of the amplitude is performed by the eikonal approach, and in the framework of the quark structure of hadrons the colour screening is taken into account. The performed description of the diffractive processes has led to the parameters of the bare pomeron P which occurred to be close to the corresponding parameters of the Lipatov's pomeron [1]. Parameters of the bare pomeron and those of the three-reggeon block PGG (G is a reggeized gluon) has been fixed by the data at moderately high energies; for superhigh energies the predictions are made. The intercept of the bare pomeron is found to be in remarkable agreement with the low-x data for deep inelastic scattering. An evaluation of the effective colour transparency radius is done which can be used in hadron-nuclei reactions.

In the latest decade the phenomenon of a pomeron attracts much attention; still, the pomeron structure remains enigmatic in many respects. A perpetual item of the agenda is the description of the pomeron in terms consistent with QCD (see, for example, ref. [2] and references therein). Although the growth of the QCD coupling constant at large distances prevents the direct use of perturbative QCD for the description of soft processes, it looks as if the pomeron, being a small-size object, provides us with an exception. In this case the bare pomeron of perturbative QCD [1,3] seems to be an appropriate object for use as a guide to the description of diffractive processes at high and superhigh energies.

The behaviour of amplitudes for hadronic diffractive processes is determined by singularities of the t-channel partial waves in the complex plane of the angular momentum j, and the singularity in the channel with vacuum quantum numbers (pomeron) dominates at high energies. The pomeron of the SU(N) Yang-Mills theory in the leading logarithmic approximation appears as a composite system of reggeizied gluons while the corresponding partial waves have

a fixed root singularity at $j = 1 + \Delta_{BFKL}$, where $\Delta_{BFKL} = (g/\pi)^2 N \ln 2$ (this is so called BFKL-pomeron[3], $\Delta \cong 0.5$ at $N = 3$). Application of QCD-pomeron in the phenomenological calculations makes it urgent to consider in the gluon ladder the virtual momenta which are close to those of the leading logarithmic approximation. In ref. [1] the virtualities of such a type have been taken into account using certain boundary condition as well as the constraint ensured by the asymptotic freedom of the SU(3) theory (QCD). The pomeron obtained in this way [1] is an infinite set of poles in the region $1 < j \leq 1 + \Delta$, and there exists a constraint on the intercept of the leading pole: $\Delta \geq 0.3$.

The dynamics of the pomeron reveals itself in the small-x deep inelastic proceses: at moderate Q^2 the structure function F_2 should behave as $x^{-\Delta}$. The global fit which is performed in ref. [4] and is based on the world data as well as on the new measurements of $F_2(ep)$ by ZEUS and H1-collaborations [5] provides the value $\Delta = 0.3$. The numerical solution of the BFKL-equation [6] mimics $x^{-0.3}$ behaviour, although it gives a bit larger value for Δ which is close to 0.5.

There are reasons to believe that a successful description of soft diffractive processes is possible with a pomeron whose characteristics are close to those of perturbative pomeron. The point is that the phenomenological pomeron used at moderately high energies for the description of the diffractive processes is an almost point-like system (see ref. [7] and references therein). This is supported by a small value of α'_P as well as by large masses of the resonances which are candidates for glueballs, $M_G \sim 1.5 \div 2.2$ GeV. As a result the integration in the gluon ladder of the pomeron is carried out over large momenta, where the running coupling constant α_s is not large. The minijet picture [8], which is successful in the description of the multiparticle production in hadron-hadron collisions, also requires comparatively large momenta in the gluon ladder.

The attempt to work with the BFKL-like pomeron but with small Δ for the description of πp and pp-scatterings at moderately high energies has been made in ref. [9]. The pomeron, being a gluon ladder (Fig. 1a), has two types of couplings with quarks of the scattered hadron: with one quark (Fig. 1b) and with two of them (the last type of coupling occurs actually via the three-reggeon vertex PGG, where P and G are pomeron and reggeized gluon, correspondingly, see Fig. 1c). These two couplings cancel each other at small interquark distances causing colour screening. The small size of the pomeron reveals itself in a small magnitude for the colour screening radius, r_{cs}, – this fact allows to understand why the additive quark model does work at moderately high energies. Moreover, colour screening effects are able to explain the deviation from additivity in $\sigma_{tot}(\pi p)$ and $\sigma_{tot}(pp)$ at $\sqrt{s} \sim 20$ GeV [9] ($\sigma_{tot}(pp)/\sigma_{tot}(\pi p) \simeq 1.6$). However, the growth of the total $pp/\bar{p}p$ cross sections at $\sqrt{s} > 30$ GeV requires the value $\Delta > 0$ [10]. Still, the value $\Delta = 0.08$, though good in fitting the data, creates problems with s-channel unitarity. To satisfy the s-channel unitarity one should take into account the rescatterings in the s-channel. This procedure does not converge at small Δ – of the order of 0.1: the more rescatterings are taken into account the larger the value of Δ needed for the input pomeron. The description of pp, πp and γp diffractive cross sections $\sigma_{tot}, \sigma_{el}, \sigma_{DD}^{single}$ and σ_{DD}^{double} presented in this paper is performed with the full set of s-channel rescatterings taken into account in the eikonal approximation. As a result, we got the value $\Delta = 0.29$: this magnitude is on the lower boarder of the constraint for the Lipatov's pomeron and coincides with the value obtained in the deep inelastic HERA experiments [5].

Further presentation is organized as follows: first of all, we give the formulae for the diffractive cross sections, then we make some comments on their derivation. The following formulae

describe total, elastic and diffractive dissociation cross sections of colliding hadrons A and B:

$$\sigma_{tot}(AB) = 2\int d^2b \int dr'\varphi_A^2(r')dr''\varphi_B^2(r'') \left[1 - \exp\left(-\frac{1}{2}\chi_{AB}(r', r'', b)\right)\right], \tag{1}$$

$$\sigma_{el}(AB) = \int d^2b \left\{\int dr'\varphi_A^2(r')dr''\varphi_B^2(r'')[1 - \exp\left(-\frac{1}{2}\chi_{AB}(r', r'', b)\right)]\right\}^2 \tag{2}$$

$$\sigma_{DD(B)}^{single}(AB) + \sigma_{el}(AB) = \int d^2b \int dr'\varphi_A^2(r')dr''\varphi_B^2(r'')d\tilde{r}'\varphi_A^2(\tilde{r}') \tag{3}$$

$$\left[1 - \exp\left(-\frac{1}{2}\chi_{AB}(r', r'', b)\right)\right]\left[1 - \exp\left(-\frac{1}{2}\chi_{AB}(\tilde{r}', r'', b)\right)\right],$$

$$\sigma_{HD}(AB) = \sigma_{el}(AB) + \sigma_{DD(A)}^{single}(AB) + \sigma_{DD(B)}^{single}(AB) + \sigma_{DD}^{double}(AB) = \tag{4}$$

$$\int d^2b \int dr'\varphi_A^2(r')dr''\varphi_B^2(r'') \left[1 - \exp(-\frac{1}{2}\chi_{AB}(r', r'', b))\right]^2.$$

The last expression, $\sigma_{HD}(AB)$, stands for full hadron diffraction. Here $dr\varphi_{A,B}^2(r)$ are the quark densities of colliding hadrons A and B which depend on the transverse coordinates:

$$dr\varphi_\pi^2(r) = d^2r_1d^2r_2\delta^2(\vec{r}_1 + \vec{r}_2)\varphi_\pi^2(r_1, r_2), \tag{5}$$

$$dr\varphi_p^2(r) = d^2r_1d^2r_2d^2r_3\delta^2(\vec{r}_1 + \vec{r}_2 + \vec{r}_3)\varphi_p^2(r_1, r_2, r_3);$$

r_i is the transverse coordinate of a quark, and the wave function squared φ_A^2 has been integrated over longitudinal variables. Proton and pion quark densities are determined using correspopnding form factors; they are presented in Appendix. The profile-function χ_{AB} corresponds to the interaction of quarks via pomeron exchange as follows:

$$\chi_{AB}(r', r'', b) = \int db'db''\delta^2(b - b' + b'')S_A(b', r')S_B(b'', r''). \tag{6}$$

Functions $S_{A,B}$ stand for the pomeron-quark interaction; they are determined by the diagrams with different couplings of the pomeron with quarks as is written below:

$$S_\pi(\vec{r}, \vec{b}) = \rho(\vec{b} - \vec{r}_1) + \rho(\vec{b} - \vec{r}_2) - 2\rho(\vec{b} - \frac{\vec{r}_1 + \vec{r}_2}{2}) \exp(-\frac{(\vec{r}_1 - \vec{r}_2)^2}{4r_{cs}^2}), \tag{7}$$

$$S_p(\vec{r}, \vec{b}) = \Sigma_{i=1,2,3}\rho(\vec{b} - \vec{r}_i) - \Sigma_{i\neq k}\rho(\vec{b} - \frac{\vec{r}_i + \vec{r}_k}{2}) \exp(-\frac{(\vec{r}_i - \vec{r}_k)^2}{4r_{cs}^2}).$$

The term $\rho(\vec{b} - \vec{r}_i)$ describes the diagram where the pomeron couples to one of the hadron quarks (Fig. 1b) while the terms proportional to $\exp(-r_{ij}^2/r_{cs}^2)$ are related to the diagram 1c with the pomeron which couples to two quarks of the hadron. This diagram is a three-reggeon graph where G is the reggeized gluon. Functions S_π and S_p tend to zero as $|\vec{r}_{ij}| \to 0$: this is the colour screening phenomenon inherent to the Lipatov's pomeron. For the sake of convenience, we perform calculations in the cms of the colliding quarks, supposing that hadron momentum is shared equally between its quarks. Then

$$\rho(b) = \frac{g}{4\pi(G + \frac{1}{2}\alpha'_P \ln s_{qq})} \exp\left[-\frac{b^2}{4(G + \frac{1}{2}\alpha'_P \ln s_{qq})}\right], \tag{8}$$

where the vertex g depends on the energy squared of the colliding quarks, s_{qq}:

$$g^2 = g_0^2 + g_1^2 \left(\frac{s_{qq}}{s_0}\right)^{\Delta}. \tag{9}$$

Such a parametrization of g^2 corresponds to the two-pole presentation of the QCD-motivated pomeron with $j_0 = 1$ and $j_1 = 1 + \Delta$. Here and below $s_0 = 1$ GeV^2.

Now let us make comments on the formulae (1)-(4). Eqs. (1)-(4) in the case of a pion beam are obtained summing the diagrams like Fig. 1d, where all the possible meson states M_i and M_j are taken into account. The assumption that a full set of meson states M_i corresponds to a full set of the quark-antiquark states leads to the diagram 1e, and just this type of diagrams with the quark intermediate states is reproduced by eqs. (1)-(4). Analogously the diagrams like Fig.1 f are taken into account in eqs. (1)-(4) in the case of a proton beam.

The diffractive cross sections (1)-(4) for a meson beam were obtained in ref. [9], while for the proton beam the final formulae were reported in ref. [11]; their derivation will be published elsewhere.

Eqs. (1)-(4) depend on the transverse coordinates of quarks, though the original expressions depend on the fractions of the momenta of the colliding hadrons carried by the quark, x_i. In the functions S we put $x_i = 1/2$ for a meson and $x_i = 1/3$ for the proton, in other words we assume that hadron wave functions $\varphi_\pi(\vec{r}, x)$ and $\varphi_p(\vec{r}, x)$ select the mean values of x_i in the interaction blocks. A wide range of wave functions obey this asumption, for example, the wave functions of quark spectroscopy. But the situation with the diagram of Fig. 1c is more complicated. One should perform an integration over the part of the energy carried by reggeized gluons and pomeron: this spreads the x_i's of the interacting quarks. However, if the intercept of the reggeized gluon $\alpha_G(0)$ is near 1 (it is actually the requirement of the BFKL pomeron), then x_i's can be considered as frozen. We have checked by numerical calculations that this assumption works at $0.8 < \alpha_G(0) < 1$ for realistic pion and proton wave functions. In due course, in eq. (9) we put $s_{qq} = s/6$ for πp collision and $s_{qq} = s/9$ for pp.

Eqs. (1)-(4) can be used at small momentum transfers where real parts of the amplitudes are small. Hence we neglected the signature factor of the bare pomeron, but it can be easily restored. We shall return to this point later on.

Eqs. (1)-(4) are written in the eikonal approximation for composite systems. It is well known that certain correlations are missed in this procedure. Let us elucidate what type of correlations is taken into account and what is neglected in the developed approach. Interactions of quarks of the same hadron and the transitions of these quarks into the excited hadron states are included in the diagrams of type 1d, and the completeness condition for the quark states results actually in multiple interactions of the "frozen" quark state (diagram of Fig. 1e). But the t-channel gluon interactions are taken into account only in their simplest form - as a set of non-interacting pomeron exchanges. Including pomeron-pomeron interactions is actually the problem of finding a solution which satisfies simultaneously both t- and s-channel unitarity conditions. Attempts to solve it have been intensified recently [12]. Calculations performed here provide arguments that eikonal diagrams with the found pomeron parameters play a decisive role in the formation of diffractive processes at present high and superhigh energies. This point will be discussed below in a more detail.

Let us discuss results of the calculation. Total and elastic pp (or $p\bar{p}$) and πp cross sections are shown in Fig. 2a, b. The parameters of the input pomeron have been obtained in the fitting

procedure in a broad energy range ($\sqrt{s} = 23.7 \div 1800$ GeV); they are as follows:

$$g_0^2 = 7.914 \text{ mb}, \quad g_1^2 = 0.179 \text{ mb}, \quad r_{cs} = 0.18 \text{ fm}; \tag{10}$$

$$\Delta = 0.29, \quad G = 0.167 \text{ (GeV/c)}^{-2}, \quad \alpha'_P = 0.112 \text{ (GeV/c)}^{-2}.$$

The wave functions φ_π and φ_p are chosen to satisfy pion and proton form factors at $|q^2| \leq 1$ GeV^2 in the framework of the quark model.

At asymptotic energies the total cross sections $\sigma_{tot}(pp)$ and $\sigma_{tot}(\pi p)$ calculated with the parameters (10) are shown in Fig. 2*a*; at superhigh energies they increase as $0.32 \ln^2 s$ mb. The growth with energy of the elastic cross sections, $\sigma_{el}(pp)$ and $\sigma_{el}(\pi p)$, calculated with eq. (2) is presented in Fig. 2*b*. At superhigh energies they grow as $0.16 \ln^2 s$ mb. Total cross sections calculated with the parameters (10) can be fitted at $\sqrt{s} \geq 100$ GeV, within 5% accuracy, by the following expressions:

$$\sigma_{tot}(pp) = 1.75 + 2.27 \ln(s/s_0) + 0.32 \ln^2(s/s_0), \tag{11}$$

$$\sigma_{tot}(\pi p) = 4.93 - 6.19 \ln(s/s_0) + 0.32 \ln^2(s/s_0).$$

and elastic cross sections can be fitted in the following form:

$$\sigma_{el}(pp) = -6.13 + 0.797 \ln(s/s_0) + 0.16 \ln^2(s/s_0), \tag{12}$$

$$\sigma_{el}(\pi p) = 3.05 - 1.38 \ln(s/s_0) + 0.16 \ln^2(s/s_0).$$

In eqs. (11) and (12) numerical coefficients are given in mb, $s_0 = 1$ GeV^2.

For LHC energy ($\sqrt{s} = 16$ TeV) our predictions, which relate to the bare pomeron parameters given by eq. (10), are as follows: $\sigma_{tot}(pp) = 131$ mb and $\sigma_{el}(pp) = 41$ mb.

The slopes B for the elastic $pp(\bar{p}p)$ and πp cross sections $d\sigma_{el}/dq^2 \sim \exp(-Bq^2)$ are shown in Fig. 2*c*: the calculated values describe well the data.

The ratio of the total cross sections $\sigma_{tot}(pp)/\sigma_{tot}(\pi p)$ tends to unity at far asymptotic energies. In this limit $\sigma_{el}(pp)/\sigma_{tot}(pp) \to 1/2$ and $\sigma_{el}(\pi p)/\sigma_{tot}(\pi p) \to 1/2$ (Pumplin's limit [14]). These limit magnitudes originate because of the disappearance of the colour screening radius at superhigh energies: effective colour screening radius, which is different for pp and πp collisions, tends to zero at asymptotic energies.

As was mentioned above, the restoration of the pomeron signature factor (or crossing symmetry of the amplitude) can be easily done, and this allows one to calculate $\rho = Re\, A/Im\, A$. The result is shown in Fig. 2*d*: the description of the data for $pp(\bar{p}p)$ collisions is rather reasonable.

Now let us discuss the process of the diffraction dissociation. First, there is a problem of the definition of σ_{DD}^{single}, for two mechanisms contribute to the measured diffractive dissociation cross section: one is the dissociation of the colliding hadron, see Fig. 3*a*, and another involves partly dissociated pomeron, Fig. 3*b*. Eqs. (3) and (4) describe the hadron dissociation only, the calculated cross section for the proton dissociation is presented in Fig. 4*a*. The difference of the measured value of $\sigma_{DD}^{single}(\bar{p}p)$ and the calculated one provides just the cross section for the partly dissociated pomeron which is determined by the three-pomeron diagram: this difference is shown in Fig. 4*b*. It should be pointed out that the developped approach allows to calculate the other characteristics of the diffraction dissociation of the colliding particles, namely, the M^2- and t-dependences. However such a study is beyond our present consideration.

In Fig. 5 the total cross section $\sigma_{tot}(\gamma p)$ is presented, together with the available experimental data obtained by ZEUS and H1 (see ref. [15] and references therein). The calculations have been performed in the framework of the hypothesis that a hadronization of the photon is governed by the vector dominance model, $\gamma \to V$, and the wave functions of the vector mesons (ρ and ω) are almost the same as for the pion, $\psi_V \simeq \psi_\pi$, under a suggestion to obey the $SU(6)$-symmetry. However, it is worth noting that total cross section is poorly sensitive to the details of the wave function. More sensitive are the two-particle reactions $\gamma p \to \rho p$ and $\gamma p \to \omega p$. In Fig. 5 we demonstrate the cross sections for these reactions calculated under the assumptions that $V = \rho + \omega$ and $\sigma(\gamma p \to \rho p) = \sigma(\gamma p \to \omega p)$.

One may be rather sceptical about the eikonalization procedure. Here we would like to present arguments why the eikonal is a good approach in a transitional region, when diffractive cross sections start to increase, reaching their asymptotic regime, $\sigma \sim \ln^2 s$. Diffractive $\log s$-physics is related to the interaction which leads to a black disk in the impact parameter space with the radius increasing as $\ln s$. The important point is that this radius is mainly determined by the interaction component which increases the most rapidly with s. Such a component is just one-pomeron exchange. The arguments are based on the fact that the growth of the pomeron interaction obtained in the description of the experimental data is strongly delayed: the parameters of the bare pomeron provide $g^2 \sim 1 + (s/3 \cdot 10^5 \cdot GeV^2)^{0.29}$.

Consider as an example the diagram where two pomerons interact with each other; then the four-pomeron block emerges but with much less energy per one pomeron, $s_i \sim ms^{1/2}$. Because of that the polynomial growth with energy of the four-pomeron block comes much later - when the black disk in the impact parameter space has been already created by one-pomeron exchanges. The black disk cannot become more black due to additional interactions: geometrical parameters of the disk and its rim have been already fixed by one-pomeron interactions, which are involved in the eikonalization procedure.

Such are the arguments why diffractive processes, which are determined by the disk geometry, can be described by the eikonal. Still, it would not be correct to declare that the four-pomeron block is not significant at superhigh energies: it is important when the diagram cutting is done, i.e. in the formation of the inclusive spectra in the central region or in multiparticle processes but not in the soft diffractive processes.

There are two important points in the log-physics when discussing the approach of the cross section to its asymptotic regime. The first one concerns the number of independent black disks which are created by the interaction before the asymptotics. In the quark model the number of disks is determined by the number of constituent quarks. At intermediate energies, when black disks are separated from each other, the screening of disks by each other is very important, and their attenuation leads to the delay of the coming $\ln^2 s$-asymptotics. Attenuation is strongly dependent on the number of interaction sources in the hadron. The second point concerns the type of attenuation – now we speak about colour screening: for example, in the squeezed quark-antiquark system the colour screening cancels the interaction totally, while the geometrical screening cancels it by one half only. This is the reason why we payed much attention to the colour screening using Lipatov's pomeron as a guide.

The idea of colour screening which is realized here on the basis of the gluon structure of the pomeron allows one to introduce the effective colour screening radius which can be applied for the calculation of a hadron-nucleus reaction in a way as it has been done in ref. [16]. For this

purpose we introduce the following colour screening profile factor (for the case of a pion beam):

$$\chi_\pi(r) = N \int d^2b dr'' \varphi_p^2(r'') \left[1 - \exp\left(-\frac{1}{2}\chi_{\pi p}(r, r'', b)\right)\right]. \qquad (13)$$

Here N is a normalization factor which is chosen to satisfy the requirement $\chi_\pi(r \to \infty) = 1$. Physical meaning of this function is simple: $\chi_\pi(r)$ describes the pion-proton interaction depending on the pion interquark distance. The concept of colour screening means a disappearance of interaction when the quarks are close to each other, namely, at the distance which is less than the colour screening radius. After the integration over impact parameter and proton coordinates, with the parameter values given in eq. (10), we got $\chi_\pi(r)$ which is presented in Fig. 6: dashed curve stands for the energy $\sqrt{s} = 546$ GeV (it should be pointed out that the calculations performed in the interval $30 < \sqrt{s} < 1800$ GeV differ very little from each other); dotted curve is calculated at far asymptotic energies $s = 10^{30}$ GeV^2; solid curve stands for $\chi_\pi(r)$ parametrized in the form $1 - \exp(-r^n/r^n_{cs,eff})$ with $n = 2.86$ and $r_{cs,eff} = 0.281$ fm.

The last item which is to be discussed here is how the calculations performed here relate to the description of the diffractive processes at moderately high energies in the framework of the one-pomeron exchange. This has been done in ref. [9] for the energy range $\sqrt{s} = 15 \div 25$ GeV where the pp-scattering amplitude has been described with the exchange of the effective pomeron; the corresponding impulse approximation diagram is shown in Fig. 7a. In the approach used in this paper the set of diagrams shown in Fig. 7b is a counterpart of Fig. 7a. In Fig. 8 the cross section related to the diagrams shown in Fig. 7b is presented depending on the energy; let us denote it as $Im\, A_{qq}$. This magnitude which can be called an effective quark-quark cross section behaves at superhigh energies as $Im\, A_{qq} \simeq \ln^2 s$. However at low energies the value $Im\, A_{qq}$ is close to the parameters found in ref. [9], namely, $Im\, A_{qq} = 6$ mb at $\sqrt{s} = 23.7$ GeV, while the magnitude found in ref. [9] is 5.5 mb. Thus, the calculation performed here is sewed rather well with the picture of the effective one-pomeron exchange used at moderately high energies.

Summing up the results of calculations we should underline that the parameters of the bare pomeron are close to those of Lipatov's pomeron [1]. They are also close to the pomeron parameters found in the low-x deep inelastic experiments [4,5].

All calculations have been performed using the program of Monte-Carlo simulation VEGAS [17].

The authors are indebted to N.A.Kivel, L.N.Lipatov and M.G.Ryskin for useful discussions. One of us (VVA) is grateful to R.S.Fletcher, T.K.Gaisser and T.Stanev for the initiating discussions and hospitality during the visit in Delaware University. This research has been supported by International Science Foundation, Grants R-10000 and R-10300.

A Proton and pion quark densities

We describe proton and pion form factors as a sum of three exponentials:

$$F_\pi = \frac{1}{8\pi^{3/2}}\left[\frac{a_\pi^2}{(2\gamma_\pi)^{3/2}}e^{-\frac{\gamma_\pi}{8}q^2} + \frac{2a_\pi^2 b_\pi^2}{(\gamma_\pi+\delta_\pi)^{3/2}}e^{-\frac{\gamma_\pi\delta_\pi}{4(\gamma_\pi+\delta_\pi)}q^2} + \frac{b_\pi^2}{(2\delta_\pi)^{3/2}}e^{-\frac{\delta_\pi}{8}q^2}\right],$$

$$F_p = \frac{1}{24\sqrt{3}(2\pi)^3}\left[\frac{a_p^2}{8\gamma_p^3}e^{-\frac{\gamma_p}{3}q^2} + \frac{2a_p^2 b_p^2}{(\gamma_p+\delta_p)^3}e^{-\frac{2}{3}\frac{\gamma_p\delta_p}{4(\gamma_p+\delta_p)}q^2} + \frac{b_p^2}{8\delta_p^3}e^{-\frac{\delta_p}{3}q^2}\right],$$

with $a_\pi = 61.052$, $b_\pi = 14.290$, $\gamma_\pi = 22.222$, $\delta_\pi = 2.533$ and $a_p = 7307.8$, $b_p = 502.4$, $\gamma_p = 11.36$, $\delta_p = 2.24$. These magnitudes correspond to the mean value of the radius squared of pion and proton: $< r_\pi^2 >= 10$ (GeV/c)$^{-2}$ and $< r_p^2 >= 17$ (GeV/c)$^{-2}$.

In the r-representation pion and proton form factors are as follows:

$$F_\pi(q^2) = \int d^2r_1 d^2r_2 \delta(r_1+r_2)\varphi_\pi^2(r_1,r_2)e^{iqr_1},$$

$$F_p(q^2) = \int d^2r_1 d^2r_2 d^2r_3 \delta(r_1+r_2+r_3)\varphi_p^2(r_1,r_2,r_3)e^{iqr_1}.$$

Here $\varphi_\pi^2 = \Sigma_{i=1}^3 A_i \exp[-a_i(r_1^2+r_2^2)]$ and $\varphi_p^2 = \Sigma_{i=1}^3 D_i \exp[-d_i(r_1^2+r_2^2+r_3^2)]$ with the parameters:

$$A_1 = 0.0080902, \quad A_2 = 0.044519, \quad A_3 = 0.10104,$$

$$a_1 = 0.045000, \quad a_2 = 0.21990, \quad a_3 = 0.39479,$$

$$D_1 = 0.00026655, \quad D_2 = 0.0015684, \quad D_3 = 0.0041892,$$

$$d_1 = 0.044401, \quad d_2 = 0.13471, \quad d_3 = 0.22502.$$

References

[1] L.N.Lipatov, Sov.Phys. JETP **63**, 904, 1986.

[2] A.Capella, J.Tranh Thanh Van, and J.Kwiecinski, Phys. Rev. Lett. **58**, 2015, 1987;
M.G.Ryskin and Yu.M.Shabelski, Z. Phys. **C56**, 253, 1992;
P.V.Landshoff, "Soft Hadron Reactions", in "QCD, 20 Years Later", vol.1,
ed. P.M.Zervas and H.A.Kastrup, World Scientific, Singapore, 1993;
R.S.Fletcher, T.K.Gaisser, and F.Halzen, Phys. Lett., **B298**, 442, 1993;
E.Gotsman, E.M.Levin, and U.Maor, Phys. Rev. **D49**, R4321, 1994.

[3] E.A.Kuraev, L.N.Lipatov, and V.S.Fadin, Sov.Phys. JETP **44**, 443, 1976;
Ya.Ya.Balitsky and L.N.Lipatov, Sov.J.Nucl.Phys. **28**, 882, 1978.

[4] A.D.Martin, W.J.Stirling, and R.G.Roberts, Phys. Rev. **D50**, 6734, 1994.

[5] ZEUS Collaboration: M.Rocco, Proc. of 29th Rencontre de Moriond, March 1994, ed. J.Tran Thanh Van;
H1-Collaboration: K.Mueller, Proc. of 29th Rencontre de Moriond, March 1994, ed. J.Tran Thanh Van.

[6] A.J.Askew, J.Kwiecinski, A.D.Martin, and P.J.Sutton, Phys. Rev. **D47**, 3775, 1993; ibid, **D49**, 4402, 1994.

[7] V.V.Anisovich, M.N.Kobrinsky, J.Nyiri and Yu.M.Shabelski, "Quark Model and High Energy Collisions", World Scientific, Singapore, 1985,
P.V.Landshoff and O.Nachtman, Z. Phys. **C35**, 405, 1987.

[8] T.K.Gaisser and T.Stanev, Phys. Lett., **B219**, 375, 1989;
M.Block, F.Halzen and B.Margolis, Phys. Lett., **B252**, 481, 1990;
R.S.Fletcher, Phys. Rev. **D46**, 187, 1992.

[9] V.V.Anisovich, L.G.Dakhno and V.A.Nikonov, Phys. Rev. **D44**, 1385, 1991.

[10] A.Donnachie and P.V.Landshoff, Nucl. Phys. **B231**, 189, 1984;
A.B.Kaidalov and K.A.Ter-Martirosyan, Sov. J. Nucl. Phys. **39**, 979, 1984.

[11] V.V.Anisovich and L.G.Dakhno, Nucl.Phys. (Proc. Suppl.) **25B**, 247, 1992.

[12] L.N.Lipatov, Phys. Lett. **B251**, 284, 1990; ibid, **B303**, 394, 1993;
J.Bartels, Phys. Lett. **B298**, 204, 1993 and "Unitarity Correction to the Lipatov Pomeron", Preprint DESY 93-028, 1993;
J.Bartels and M.G.Ryskin, Z. Phys. **C56**, 1751, 1993.

[13] M.G.Albrow et al.,Nucl. Phys. **B108**, 1, 1976;
S.Belforte, G.Chiarelli, P.Giromini, S.Miscetti and R.Paoletti, "Measurement of Small Angle Antiproton-Proton Elastic Scattering at $\sqrt{s} = 546$ and $\sqrt{s} = 1800$ GeV", Preprint CDF/ANAL/CDF/CDFR 2049, 1994;
S.Belforte, G.Chiarelli, P.Giromini, K.Goulianos, S.Miscetti and R.Paoletti, "Measurement of $\bar{p}p$ Single Diffraction Dissociation at $\sqrt{s} = 546$ and $\sqrt{s} = 1800$ GeV", Preprint CDF/ANAL/CDF/CDFR 2050, 1994;
S.Belforte, G.Chiarelli, P.Giromini, S.Miscetti and R.Paoletti, " Measurement of the Antiproton-Proton Total Cross Section at $\sqrt{s} = 546$ and $\sqrt{s} = 1800$ GeV", Preprint CDF/ANAL/CDF/CDFR 2051, 1994.

[14] J.Pumplin, Phys.Rev. **D8**, 2899, 1973.

[15] N.A.Pavel (ZEUS collaboration), "New results from ZEUS", Preprint DESY 93-160, 1993;
G.Wolf, "HERA Physics", Preprint DESY 94-022, 1994.

[16] V.V.Anisovich, L.G.Dakhno, V.A.Nikonov and M.G.Ryskin, Phys. Lett. B292, 169, 1992;
V.V.Anisovich, L.G.Dakhno and M.M.Giannini, Phys. Rev. **C49**, 3275, 1994.

[17] G.P.Lepage, J.Comp. Phys. **27**, 192, 1978.

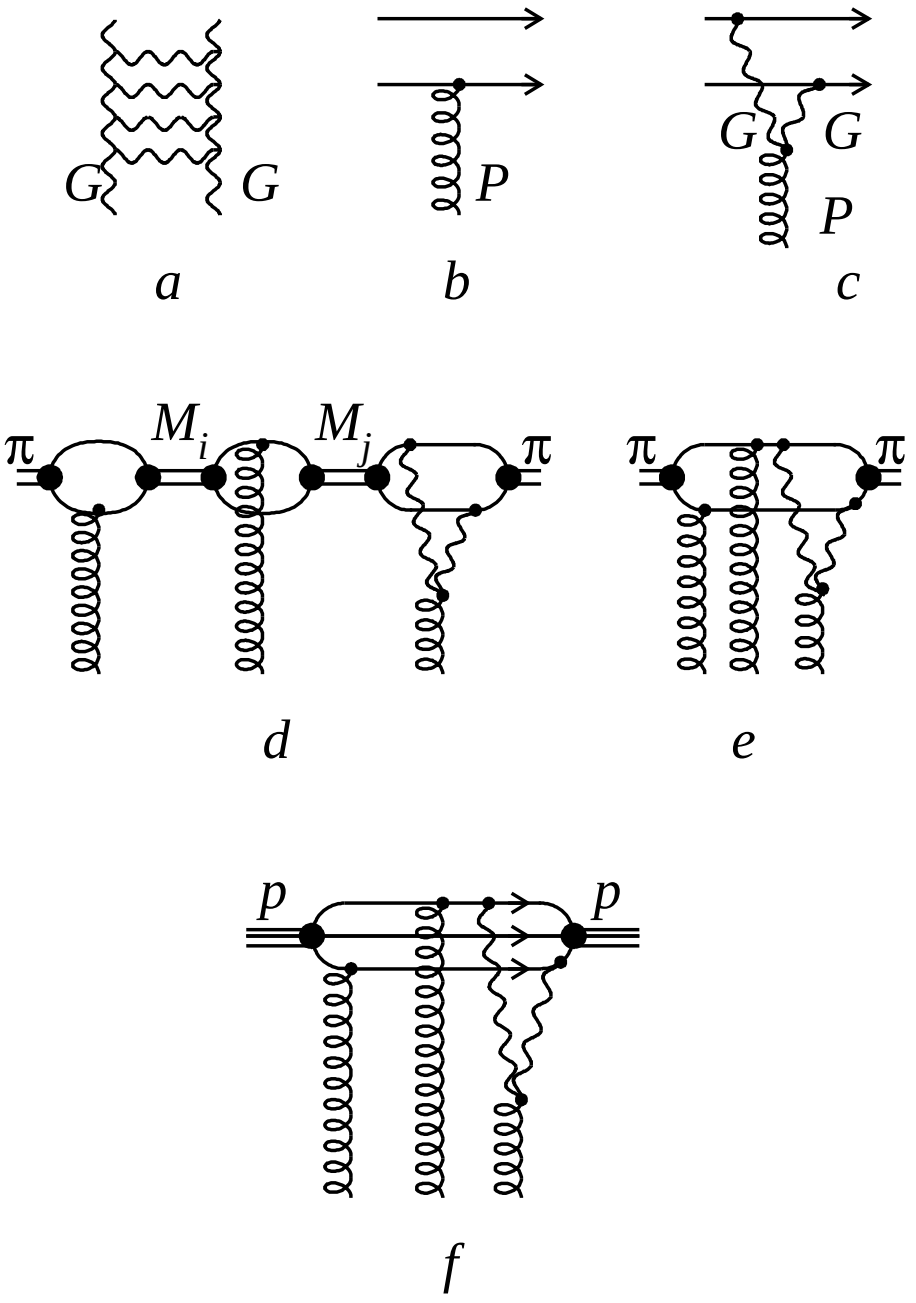

Fig. 1. a) Gluon ladder diagram of the Lipatov's pomeron; b, c) various types of pomeron-quark couplings; d) diagrams of soft multiple rescatterings for the pion beam written using the language of hadron intermediate states; the summation is performed over all allowed meson states M_i and M_j; e) the same diagrams as in fig. $1d$ but written in the language of quark rescatterings; f) the same as Fig. $1e$, but for the proton.

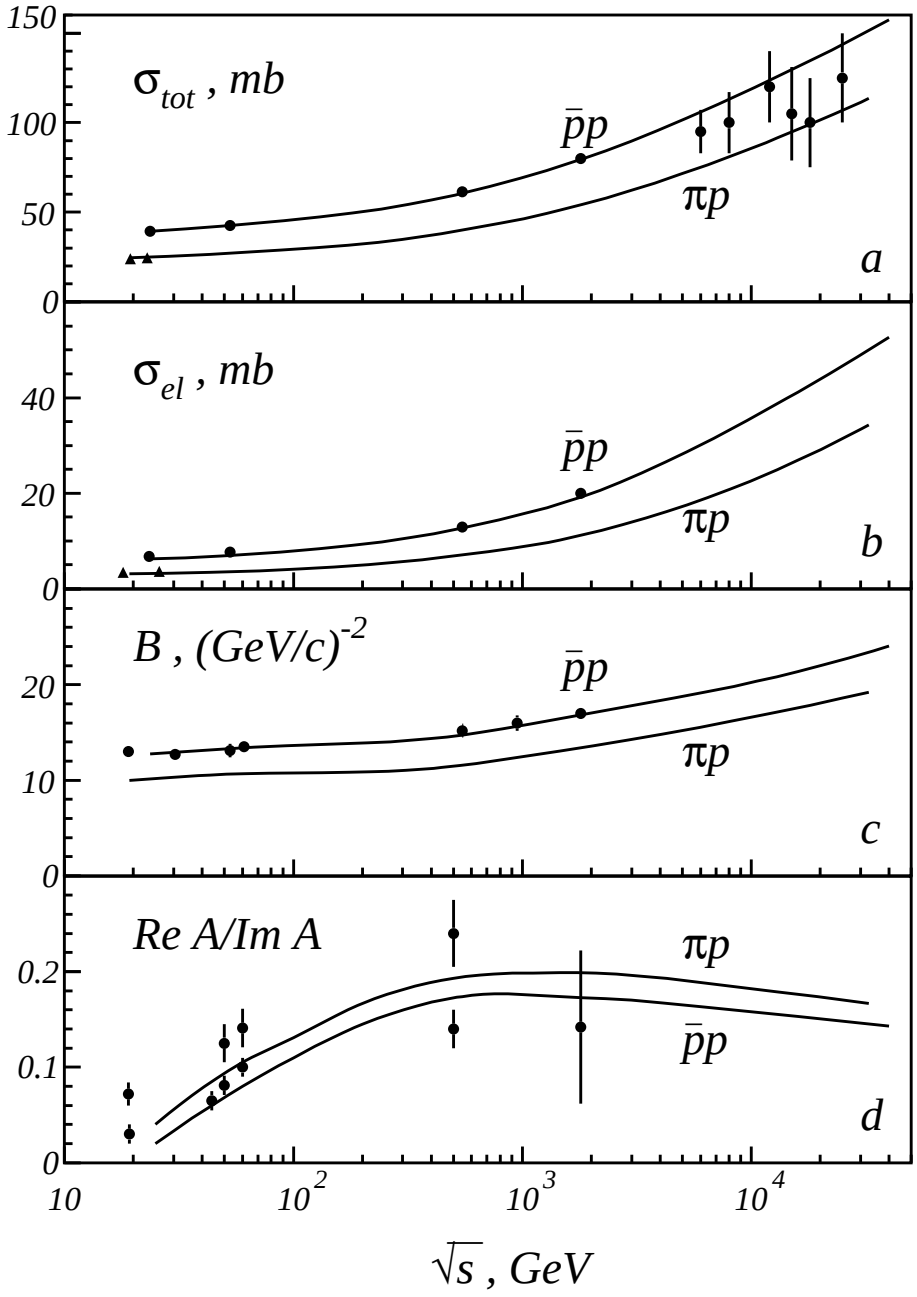

Fig. 2. Experimental data and calculated values for $pp(\bar{p}p)$ and πp collisions: a) total cross sections, the data at $\sqrt{s} > 5000$ GeV are Akeno cosmic ray experiment; b) elastic cross sections; c) slope parameter the elastic scattering; d) $\rho = Re\,A/Im\,A$ for $pp(\bar{p}p)$ and πp scattering.

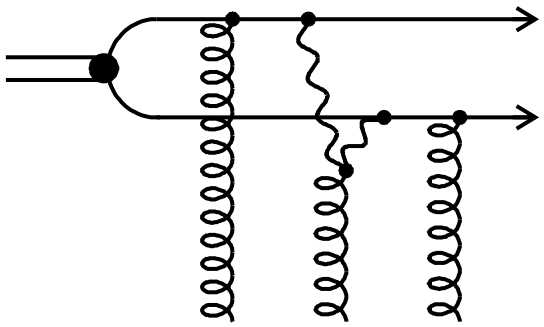

a

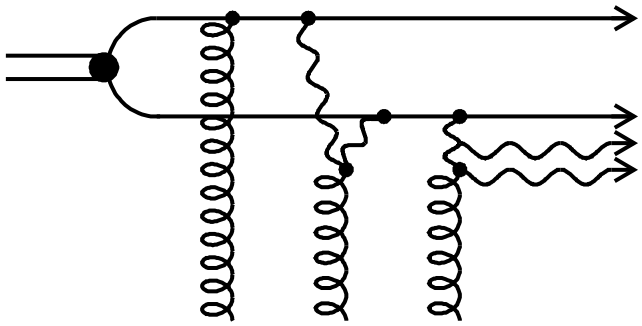

b

Fig. 3. Examples of DD processes which are measured in the experiments: *a*) The dissociation of hadron, *b*) Process with the partly dissociated pomeron - this process has not been taken into account in eqs. (3)-(4).

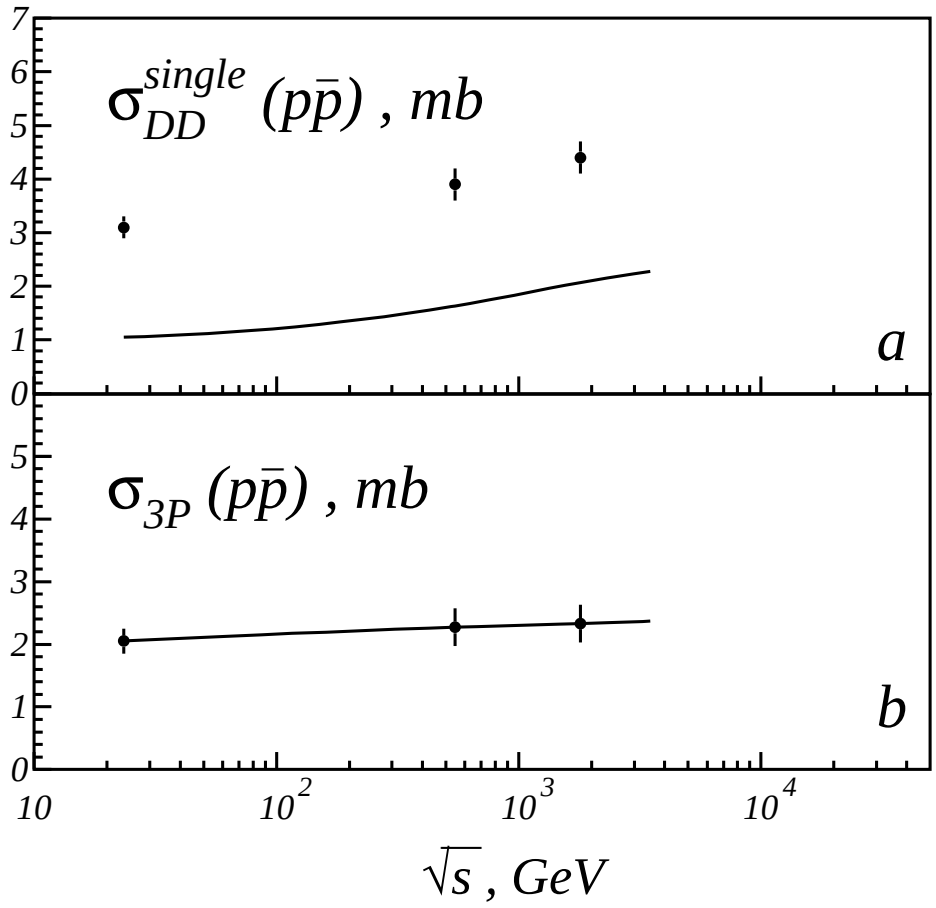

Fig. 4. *a*) Experimental data for the proton diffraction dissociation in $p\bar{p}$ collisions [13] measured as $\sigma_{DD}(exp) = \int dM^2 d\sigma/dt dM^2,\ 0 < -t < 0.4,\ M^2/s < 0.15$; curve presents the values of $\sigma_{DD}^{single}(pp)$ calculated by eq. (3). *b*) Cross section of the diffraction dissociation of the pomeron evaluated as $\sigma_{3P}(pp) = \sigma_{DD}(exp) - \sigma_{DD}^{single}(pp)$; curve is a parametrization of the three-pomeron diffractive cross section in the form $(1.85 + 0.033 \ln s/s_0)$ mb.

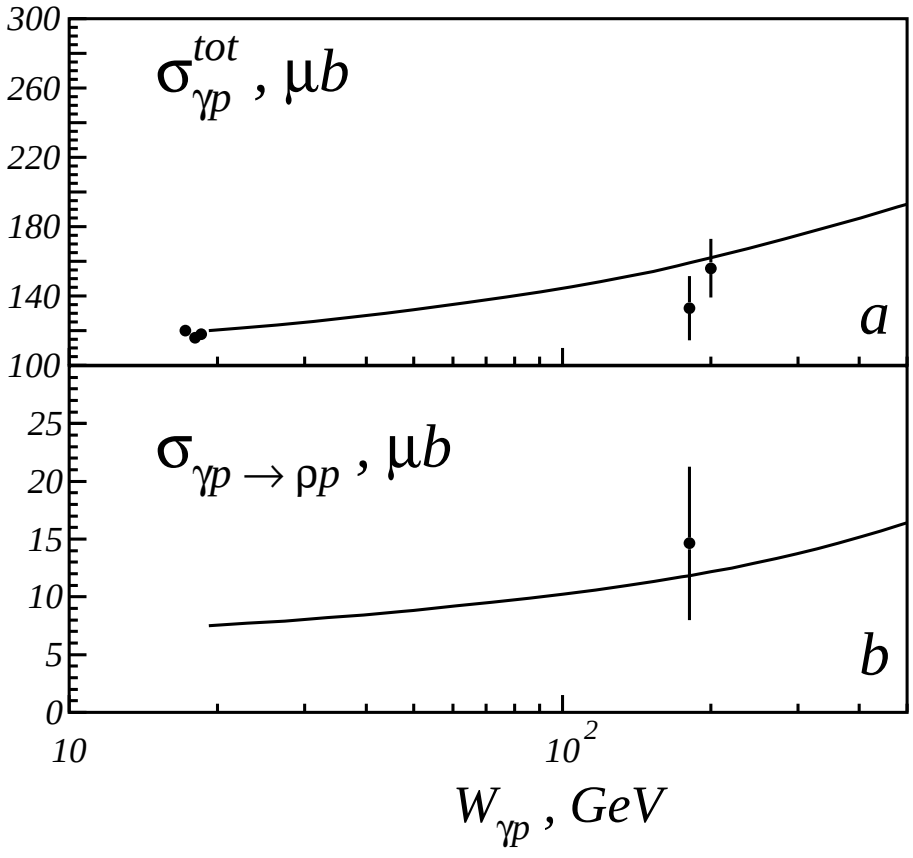

Fig. 5. a) Total cross section $\sigma_{tot}(\gamma p)$ calculated by eq. (1) (solid curve) and b) cross section for the two-particle reaction $\sigma_{tot}(\gamma p \to \rho p)$ calculated by eq. (2).

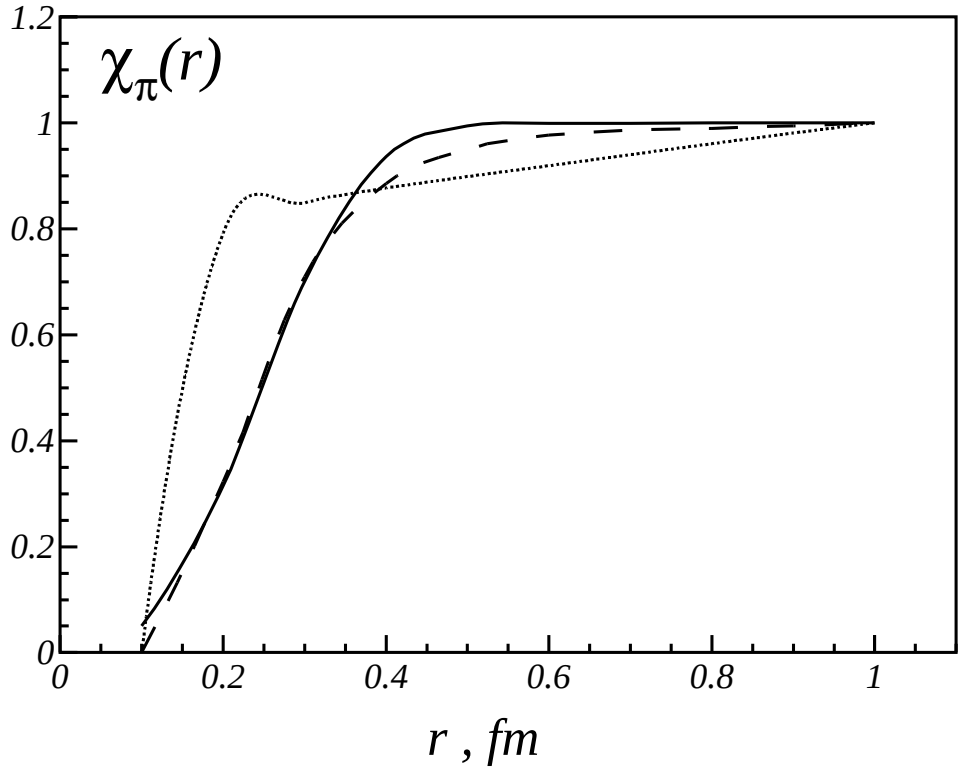

Fig. 6. Colour screening profile factor $\chi_\pi(r)$ as a function of the interquark distance (for pion-proton collision). Dashed curve stands for the energy $\sqrt{s} = 546$ GeV; dotted curve is calculated at far asymptotic energies $s = 10^{30}$ GeV^2; solid curve stands for $\chi_\pi(r)$ parametrized in the form $1 - \exp(-r^n/r^n_{cs,eff})$ with $n = 2.86$ and $r_{cs,eff} = 0.281$ fm.

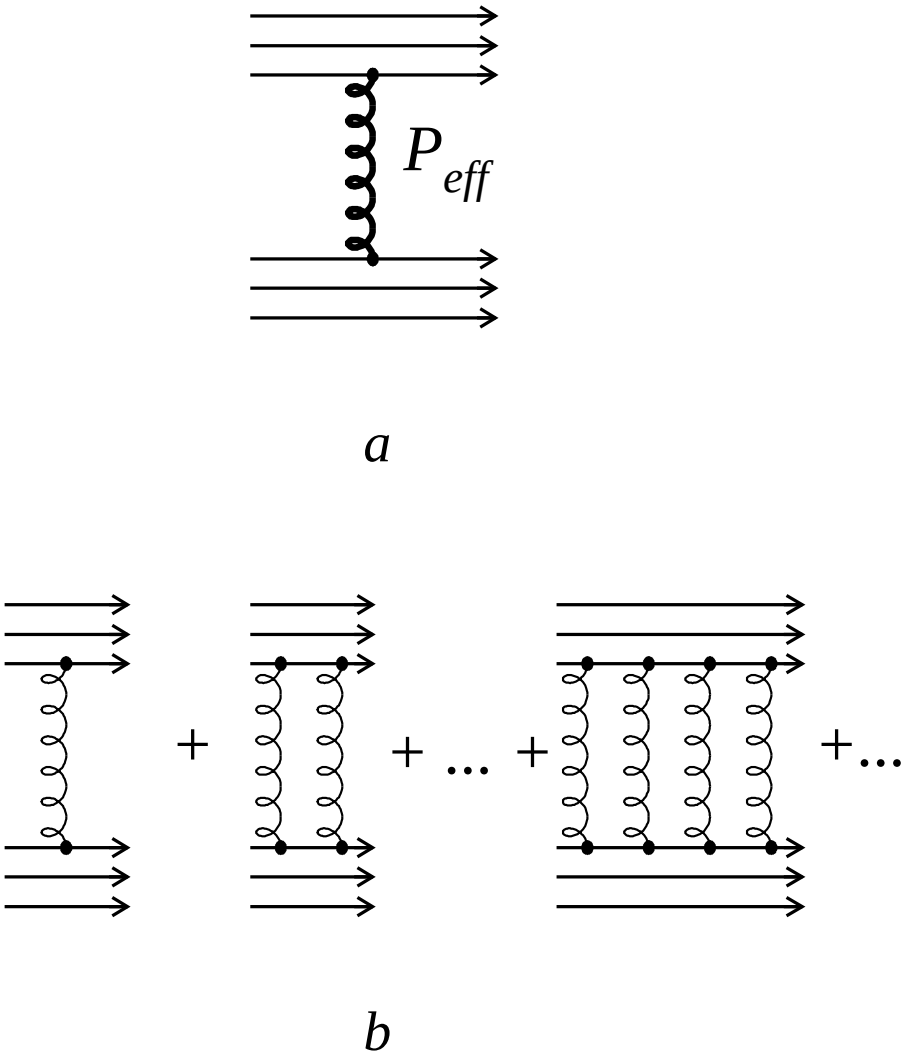

Fig. 7. Impulse approximation diagrams: *a*) Exchange of the effective pomeron in the *pp*-collision which was used in ref. [9]; *b*) Eikonal approximation diagrams for the quark-quark interaction which play the role of the effective pomeron at moderately high energies.

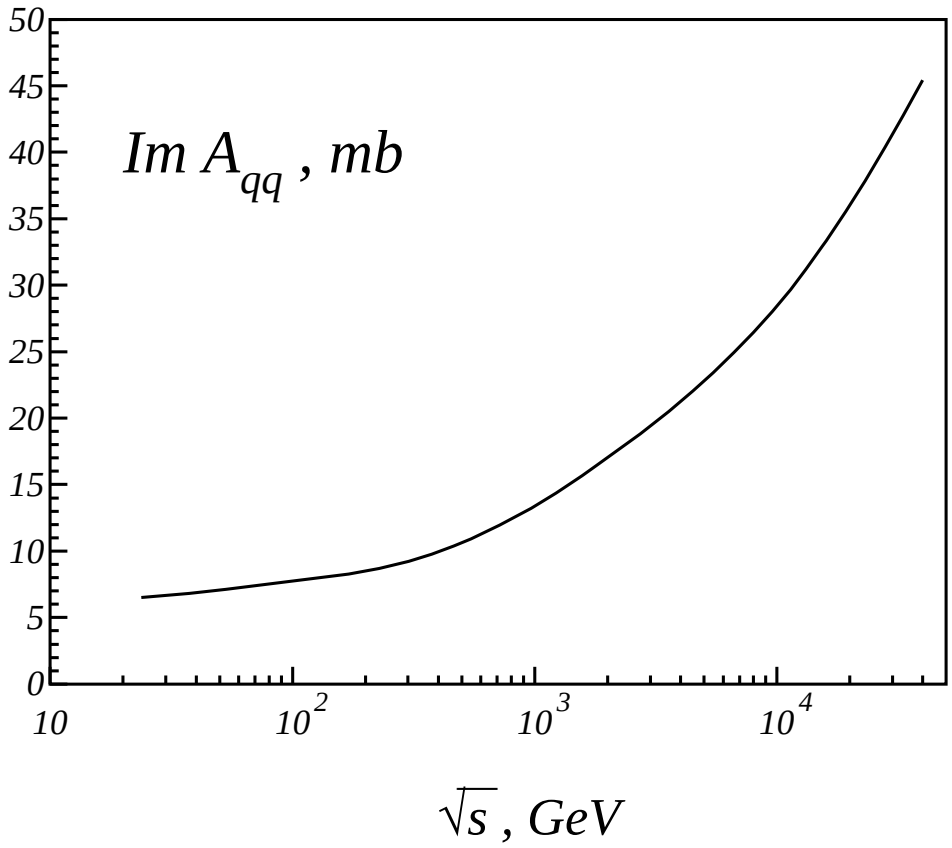

Fig. 8. Energy dependence of the cross section related to the set of diagrams shown in fig. 7*b*.